

# Dynamically Modulating the Surface Plasmon Resonance of Doped Semiconductor Nanocrystals

Guillermo Garcia,<sup>†,‡</sup> Raffaella Buonsanti,<sup>†</sup> Evan L. Runnerstrom,<sup>†,§</sup> Rueben J. Mendelsberg,<sup>†,||</sup> Anna Llordes,<sup>†</sup> Andre Anders,<sup>||</sup> Thomas J. Richardson,<sup>†</sup> and Delia J. Milliron<sup>\*,†</sup>

<sup>†</sup>The Molecular Foundry, Lawrence Berkeley National Laboratory, Berkeley, California 94720, United States

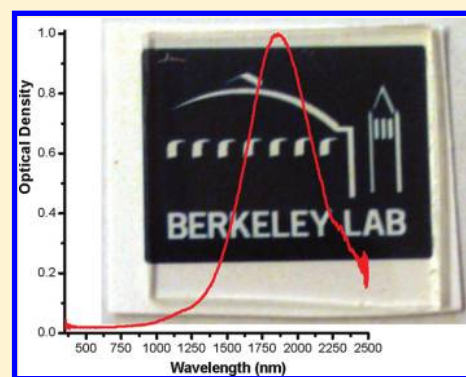
<sup>‡</sup>Department of Mechanical Engineering and <sup>§</sup>Department of Materials Science and Engineering, University of California, Berkeley, California 94720, United States

<sup>||</sup>Plasma Applications Group and <sup>†</sup>Environmental Energy Technologies Division, Lawrence Berkeley National Laboratory, Berkeley, California 94720, United States

**S** Supporting Information

**ABSTRACT:** Localized surface plasmon absorption features arise at high doping levels in semiconductor nanocrystals, appearing in the near-infrared range. Here we show that the surface plasmons of tin-doped indium oxide nanocrystal films can be dynamically and reversibly tuned by postsynthetic electrochemical modulation of the electron concentration. Without ion intercalation and the associated material degradation, we induce a > 1200 nm shift in the plasmon wavelength and a factor of nearly three change in the carrier density.

**KEYWORDS:** Surface plasmon, nanocrystal, indium tin oxide, spectroelectrochemistry, doping



Localized surface plasmon resonance (LSPR) features of metallic nanostructures have been leveraged for sensors, surface enhanced spectroscopy, and light-trapping in photovoltaic cells.<sup>1–5</sup> Unlike metals, plasmon resonance frequencies of doped semiconductors can be modified by changing the material's composition, creating new opportunities for plasmonic manipulation of light. In fact, well-defined LSPR features have recently been observed in the optical (infrared) spectra of highly doped semiconductor nanocrystals (NCs), especially transparent conducting oxides such as tin-doped indium oxide (ITO).<sup>6–8</sup> These optical characteristics are of great interest since the position of the plasmon peak can be adjusted on the basis of the chemical doping level. However, chemical tuning of the plasmon is fixed by the composition of the material, which cannot generally be dynamically modified. While it was shown very recently that the LSPR of copper deficient Cu<sub>2</sub>S and Cu<sub>2</sub>Se NCs shifts in response to oxidizing or reducing chemical treatments, this composition-driven optical response relies on the unusually high mobility of Cu<sup>+</sup> ions and the mechanisms for reversing oxidative doping remain uncertain.<sup>9,10</sup>

Here, we show that the surface plasmon resonance of ITO NC films can be dynamically tuned through fully reversible electrochemical doping, hence realizing the promise of electrical manipulation of semiconductor LSPR features. Electrochemical doping of CdSe NC films was previously shown to bleach the exciton peak at the onset of the visible band gap absorption and to introduce a new intraband absorption peak in the far-infrared

region.<sup>11,12</sup> However, the LSPR modulation of our ITO NCs is a collective response of the free electrons, more analogous to the electrochemical response of Au or Ag LSPR.<sup>13,14</sup> In such metal nanostructures, acute screening by a high-background charge density limits the shift of the LSPR peak to 10 or 20 nm, at most. Here, we show that the ITO NC LSPR can shift dynamically across a range covering much of the near-infrared (NIR) spectrum (including telecommunications wavelengths), opening the door to potential applications including controlling optical coupling into or out of nanoplasmonic devices or tuning plasmonic enhancement of spectroscopic signatures.<sup>15</sup> In this report, we elucidate the potential for these films to dynamically modulate transmittance of solar infrared radiation. Considering their excellent visible transparency, such modulation offers a unique opportunity for a dynamic coating on advanced, energy-saving “smart windows.”

To prepare these coatings, we first synthesized colloidal ITO NCs of variable size and doping level by balancing precursor reactivity and adjusting the indium and tin content in the feedstock (Figure 1a–d, Supporting Information Figure S1, S2, and Table S1). Our modifications of literature procedures<sup>6,7</sup> are described in the Supporting Information. The resulting NCs are capped with organic ligands that facilitate dispersion in hydrophobic solvents. Transmission spectra of these dispersions

**Received:** July 28, 2011

**Published:** August 22, 2011

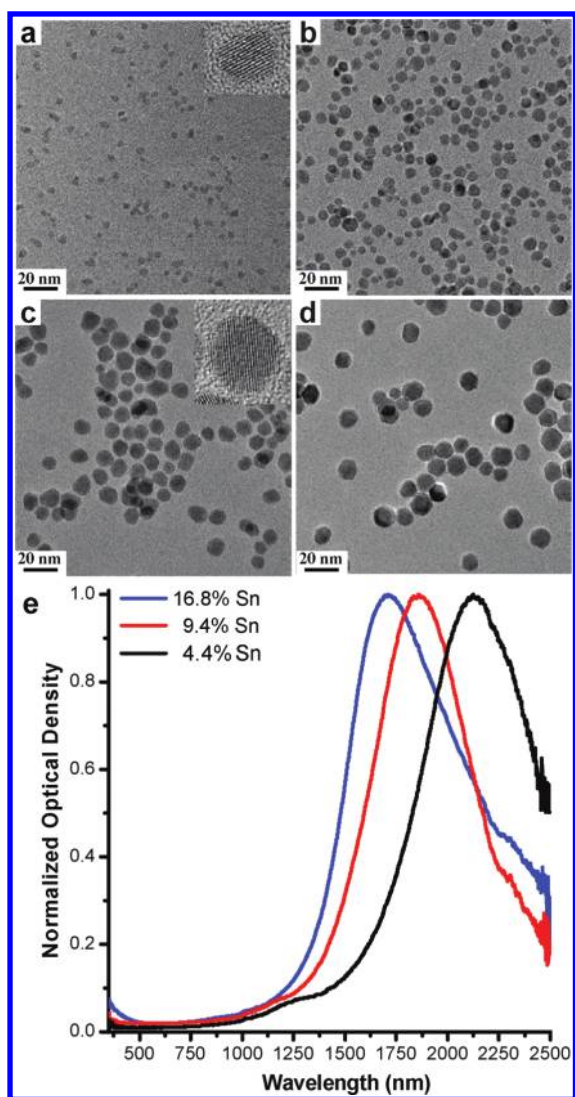


**Figure 1.** Transmission electron microscopy images of ITO NCs of varying size (nm): (a)  $4.1 \pm 0.6$ , (b)  $7.4 \pm 1.4$ , (c)  $10.2 \pm 1.7$ , and (d)  $12.1 \pm 1.5$ . (e) Extinction spectra of NCs with varying tin content (%) in solvent dispersions.

reveal well-defined LSPR peaks whose position relates to the doping level (Figure 1e). The frequency of the LSPR ( $\omega_{\text{LSP}}$ ) is proportional to the bulk plasmon frequency ( $\omega_{\text{p}}$ ), which varies as the square root of the free carrier concentration ( $n$ ).<sup>1</sup>

$$\omega_{\text{LSP}} \propto \omega_{\text{p}} = \sqrt{\frac{ne^2}{m^* \epsilon_0}} \quad (1)$$

Here, our synthetic variation of the tin content manipulates  $n$ , which in turn adjusts  $\omega_{\text{LSP}}$ . The LSPR resonance frequency varies much less strongly with size,<sup>1</sup> which is therefore available as a pseudoindependent variable in tuning the properties of our active coatings.

To enable dynamic modulation of the LSPR, the NCs were processed into electrically conducting films, approximately 150 nm thick (Figure 2a). Deposition of uniform, nonscattering films by spin coating from a mixture of hexane and octane was facilitated by the hydrocarbon ligands which cap the surfaces of the NC. However, these ligands form highly insulating barriers

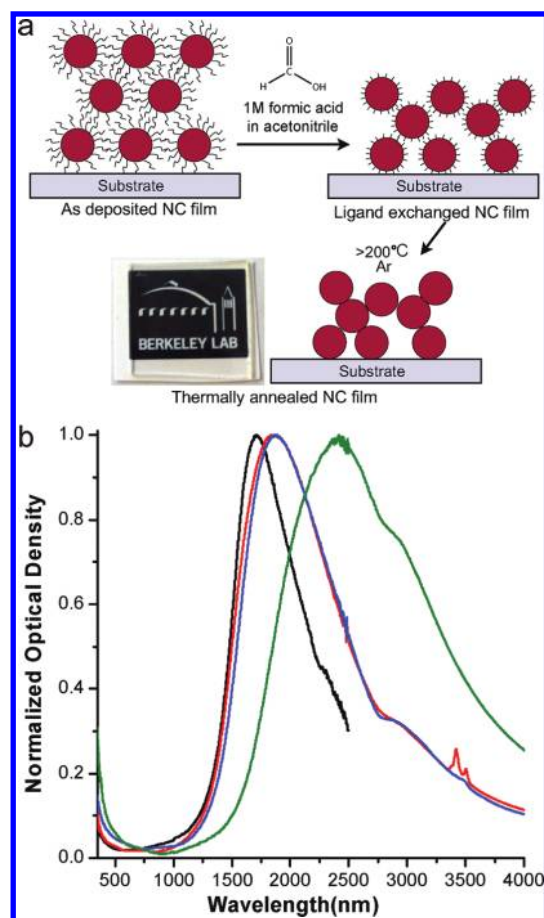


**Figure 2.** Processing NCs (4.1 nm diameter, 16.8% Sn) into conducting films. (a) Schematic of the process and photo of resulting film on quartz. (b) Optical spectra of ITO NCs in tetrachloroethylene dispersion (black), a film as-deposited (red), a film after formic acid ligand exchange (blue), and following 250 °C annealing in argon (green). Data points <2500 nm represent visible–NIR spectra, using quartz substrates, while those >2500 nm are taken from FTIR spectra on silicon substrates. Note that peaks due to C–H bond stretching at  $3500 \text{ cm}^{-1}$  are eliminated by the ligand exchange process.

between adjacent NCs and must be eliminated. Simple air annealing caused the LSPR feature to disappear, consistent with the trapping of free carriers by filling structural oxygen vacancies.<sup>16</sup> Instead, we displaced the original, bulky oleic acid ligands with small molecules by submerging the NC film in a solution of formic acid, resulting in mass-action driven ligand exchange within the film.<sup>17</sup> Formic acid is volatile and can be desorbed by low-temperature annealing in an inert environment (Supporting Information Figure S3). The sheet resistance of the film drops with annealing temperature up to 500 °C, but it is already sufficiently low following a 200 °C anneal to conduct in-plane over centimeter-scale sample dimensions (Supporting Information Figure S4). For subsequent investigations, we annealed the films at 250 °C, which reproducibly gave well-conducting films with a low thermal budget.

At each stage of film deposition and processing, the absorption peak shifted to longer wavelength (Figure 2b), raising questions about possible changes in the free carrier concentration and the structure of the NC films. First, we verified that the crystallite size remains fixed; the X-ray diffraction pattern and peak widths remain

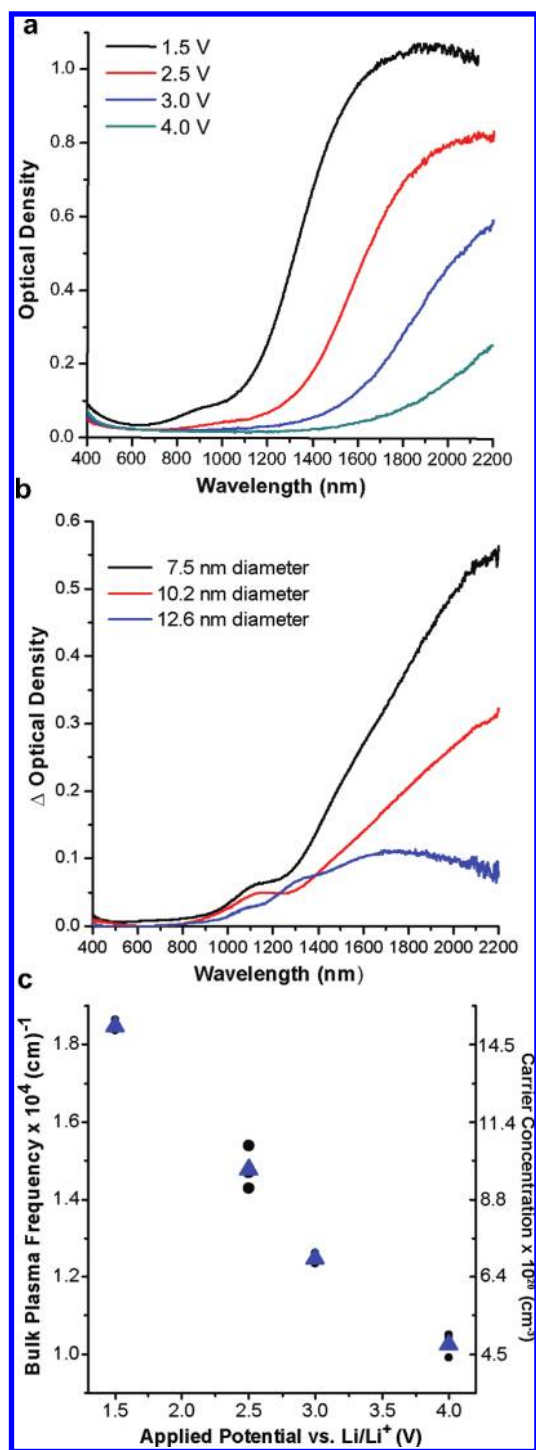


**Figure 3.** Optical properties of ITO NC films during electrochemical modulation. (a) Bias-dependent optical density of a film composed of 4.1 nm diameter, 16.8% Sn NCs. (b) Change in optical density between 1.5 and 4 V for various NC sizes, each with  $4.65 \pm 0.25\%$  Sn. (c) Plasmon frequency ( $\omega_p$ ) and carrier concentration ( $n$ ) versus applied potential, derived from the results in (a). Circles show results of fitting using various starting conditions while blue triangles show average values. All potentials are referenced to a  $\text{Li}/\text{Li}^+$  electrode in 0.1 M  $\text{LiClO}_4$  in propylene carbonate.

unchanged following annealing (Supporting Information Figure S5). Next, we employed an extended Drude model to fit the optical

transmission spectra. The model (discussed more extensively in the Supporting Information) considers possible changes in the carrier concentration, the dielectric environment, the volume fraction of the NCs, as well as variations in damping that might arise as the NC surfaces are chemically modified.<sup>18,19</sup> Excellent fits are achieved to the experimental data (Supporting Information Figure S6) from which we conclude that the shifts in the absorption peak can be primarily ascribed to an increasing ITO volume fraction from extremely low in the solvent dispersion, to 0.35 in the as-deposited film containing oleic acid ligands, and finally to 0.47 in the ligand exchanged and annealed film (Supporting Information Table S2). The increasing ITO volume fraction both enhances coupling between adjacent NCs, which are brought into more intimate contact with each other during processing and raises the average dielectric environment surrounding the NCs.<sup>20,21</sup> Notably, there is very little change in the plasmon frequency, and therefore in the free carrier concentration, during film processing.

To actively modulate their surface plasmon resonance, the NC films were positioned as the working electrode in an electrochemical cell and in situ transmission spectra recorded as a function of the applied potential. Because of the onset of strong absorption bands of the electrolyte, the in situ measurements were limited to a spectral window of 400–2200 nm. The optical spectrum of the film at its open circuit voltage shows minimal change compared to its spectrum in an air environment, consistent with the change in dielectric environment and indicating that no chemical reactions occur at the NC surface (Supporting Information Figure S7). As we apply a negative bias, the SPR peak shifts to higher energy and becomes more intense (Figure 3a). Both changes are consistent with the modulation of the free carrier concentration,  $n$ , which would shift the plasmon resonance frequency, as in eq 1, and increase the extinction at the LSPR peak proportionally.<sup>1</sup> This result stands in stark contrast to earlier reports of the spectroelectrochemical response of nanocrystalline Sb-SnO<sub>2</sub> films.<sup>22,23</sup> In that case, the applied potential induced negligible shift, only changing the intensity of the plasmon absorption feature. It was suggested that a high density of surface traps led to a strong depletion of free carriers near the surface and a variation in the thickness of this depletion region was proposed to account for the nearly constant  $\omega_{\text{LSP}}$  even as electrons were injected or extracted. The strong shifting of the LSPR peak we observe suggests that our ITO NC films are relatively free of such surface defect sites.

In fact, we propose that the modulation of the surface plasmon resonance in our ITO NC films is more analogous to that found in metallic nanostructures<sup>14</sup> and is related to that demonstrated recently at the planar interface of ITO with a dielectric layer.<sup>24</sup> In the latter case, the free carrier concentration in a thin ( $\sim 5$  nm) accumulation region was modulated by applying a potential between the ITO film and a counter electrode on the opposite side of the dielectric layer. Since we observe plasmon resonance shifts to both shorter and longer wavelength than the initial state, we suggest that accumulation and depletion regions, respectively, are formed near the surface of the NCs. This hypothesis predicts greater modulation for smaller NCs, whose entire volume can lie within the strongly modulated accumulation/depletion region. Indeed, comparing NCs of similar chemical doping level, the magnitude of the change in extinction between the two extremes of applied bias tracks with NC diameter (Figure 3b). Thus, for small, highly doped NCs we can strongly modulate the

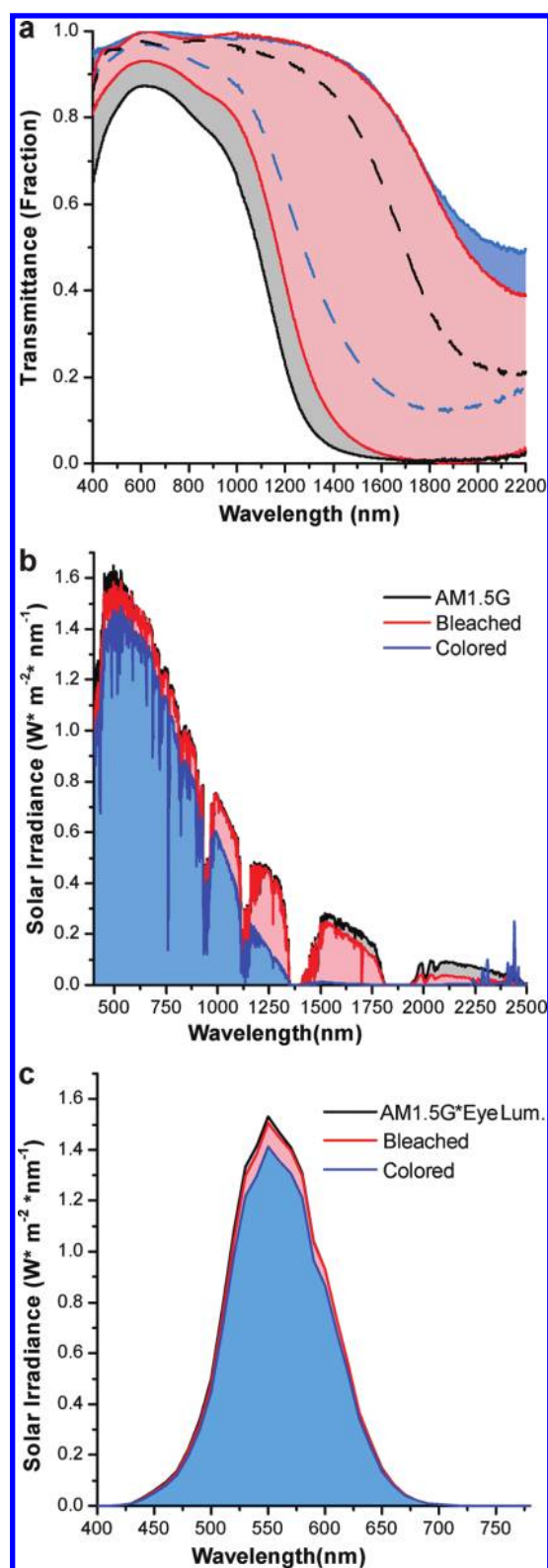


**Figure 4.** Analysis of film performance as a dynamic, spectrally selective window coating. (a) Transmission spectra at 1.5 (bleached) and 4 V (colored) for various film thickness (150, 310, and 460 nm shown in blue, red, and black, respectively) of 4.5 nm, 16.9% Sn NCs. (b) The portion of the AM 1.5G solar spectrum transmitted in the bleached and colored states of the 310 nm thick film. (c) Comparison between the AM 1.5G luminous solar spectrum and the luminous solar transmittance for the bleached and colored states.

plasmon frequency, and the associated free carrier concentration, throughout the volume of each NC and of the overall film.

We can quantitatively evaluate these dynamic changes by fitting the spectra of the electrochemically modulated NC film using the extended Drude model (again, discussed in the Supporting Information). Absolute transmittance of the entire electrochemical cell is used for the modeling in order to properly account for the interfaces. For the free parameters associated with the ITO nanocrystal film, confidence in the values was evaluated by starting with various initial conditions and keeping all parameters within physically reasonable bounds. We found that  $\omega_p$  converged reliably to near the same value regardless of the starting conditions, so that  $\omega_p$  and  $n$  could be extracted as a function of the bias applied in the electrochemical cell (Figure 3c and Supporting Information Figure S8). The free carrier concentration changes by nearly a factor of 3, resulting in almost a factor of 2 change in the plasmon frequency between the two extremes.

Such large changes in plasmon resonance could be applicable to micrometer-scale plasmonic devices, or might even be leveraged at the single-nanocrystal level.<sup>2,14</sup> Unlike the case of a planar ITO film, the transmission through the NC film changes dramatically since there is far greater surface area. We note that the contrast ratio for transmittance of 1.55  $\mu\text{m}$  light, relevant to telecommunications, exceeds 12:1 ( $\sim 11$  dB) without any optimization. By adjusting the chemical doping level, modulation of any specific wavelength in the NIR could be maximized.

The electrochemical modulation of transmittance through thin films, as demonstrated here, is of particular interest for dynamic “smart window” applications. In this case, the NC film is effectively part of a macroplasmonic device, operating on nanoplasmonic principles. The heat load derived from solar infrared radiation could be dynamically modulated in response to the changing outdoor environment, while visible light transmittance is maintained for daylighting use.<sup>25</sup> In contrast, the conventional electrochromic window coatings reported in the literature and now emerging on the market most strongly modulate visible light, with a more modest dynamic range for NIR transmittance.<sup>26</sup>

In order to explore the potential performance of a dynamic, spectrally selective window coating based on LSPR modulation, we measured the dynamic transmittance of NC films as a function of film thickness (Figure 4a). In thicker films the surface plasmon absorption becomes saturated, providing a sharper edge between high and low transmission and minimizing the NIR transmittance at negative bias. However, the maximum NIR transmittance at positive bias and the visible transmittance, in general, are adversely affected. These trade-offs lead to an optimal thickness at which the dynamic range of NIR transmittance is maximized, with minimal impact on visible transmittance.

The implications of these dynamic optical properties for smart window performance can be evaluated by convoluting the transmittance spectra of the 310 nm thick NC film with the solar spectrum (Figure 4b). The shaded regions show the portion of the solar spectrum transmitted when the film is in the “bleached” state (positive bias) and “colored” state (negative bias). It is apparent that NIR light is strongly modulated while visible light is largely transmitted in both states. Integrating these curves, we find a 21% difference in transmittance overall and 35% difference in transmittance of the NIR portion of the solar spectrum between the two states. This already represents a substantial modulation of solar heating for a window, with further gains potentially available by additional optimization of

nanocrystal size, chemical doping level, coupling, and film thickness. Meanwhile, there is only 6% modulation of the solar insolation visible to the human eye (Figure 4c); even in the colored state, over 92% of this light remains available to offset the need for electric lighting.

An important requirement of plasmonic switching, whether applied to macro- or microscale devices, is stability under repeated cycling. In fact, this is a critical factor limiting the application of many otherwise promising electrochromic technologies to smart window coatings.<sup>26</sup> Preliminary durability testing of our NC films shows virtually no change in their electrochemical properties over multiple charge–discharge cycles (Supporting Information Figure S9), and CdSe NC films have been cycled at least 10 000 times without degradation.<sup>12</sup> The stability of our films is consistent with the mechanism proposed above in which an accumulation/depletion layer is reversibly switched near the NC surface. Unlike a conventional electrochromic coating<sup>26</sup> or the plasmonic Cu<sub>2</sub>S and Cu<sub>2</sub>Se NCs recently reported,<sup>9,10</sup> this operating principle does not involve cation migration through the active material. In other words, the switching is capacitive and our coating operates like the electrode of a supercapacitor whereas conventional electrochromic films are more analogous to battery electrodes.

The hypothesis of capacitive switching was tested by comparing the spectroelectrochemical response of a NC film in Li<sup>+</sup> containing electrolyte (used in all the experiments described thus far) to its behavior in a tetrabutylammonium (TBA<sup>+</sup>) electrolyte. Unlike Li<sup>+</sup>, TBA<sup>+</sup> is physically too large to intercalate, leaving only capacitive contributions.<sup>23</sup> The charging profile recorded by cyclic voltammetry is similar for the two electrolytes, and the total charge injected and extracted is nearly identical (Supporting Information Figure S10). Even more telling, the NIR optical responses are indistinguishable (Supporting Information Figure S11). Clearly, intercalation is not required to achieve the extreme modulation of plasmon resonance that we observe. A principle degradation pathway for battery and electrochromic electrode materials, namely strain from repeated intercalation and deintercalation,<sup>26</sup> is thus completely circumvented by the capacitive operating mechanism. The coloration efficiency is also improved by several fold over conventional electrochromic films (Supporting Information Figure S12).

The efficacy of compensating injected carriers capacitively, without intercalation, is not limited to the choice of ITO as an electrode material; it is rather a direct consequence of nanostructuring on the single-digit nanometer scale. Any material that undergoes a change in optical properties upon charging and discharging, including other plasmonic NCs but also conventional electrochromic materials like WO<sub>3</sub>, could in principle be operated in this manner.<sup>27</sup> Hence, our results suggest a new paradigm for the design of nanocrystal-based electrochromic electrodes that are robust to cycling, greatly expanding options for material selection to achieve targeted optical response characteristics for smart windows and other applications of optical modulation.

## ■ ASSOCIATED CONTENT

Supporting Information. Materials and methods, description of Drude modeling, Figures S1–S12, and Tables S1 and S2. This material is available free of charge via the Internet at <http://pubs.acs.org>.

## ■ AUTHOR INFORMATION

### Corresponding Author

\*E-mail: [dmilliron@lbl.gov](mailto:dmilliron@lbl.gov).

## ■ ACKNOWLEDGMENT

We acknowledge helpful discussions with Ms. T. Mattox and Drs. J. Urban P. J. Schuck, and R. Zuckermann. Research was supported by the U.S. Department of Energy (DOE) under Contract No. DE-AC02-05CH11231, including work performed at the Molecular Foundry as a user project, support from the Laboratory Directed Research and Development Program (Drs. Buonsanti, Mendelsberg, Llordes, Anders, and Richardson), and a DOE Early Career Research Program grant (Mr. Garcia and Dr. Milliron). Mr. Runnerstrom was supported by a Chancellor's Fellowship for Graduate Study. G.G., R.B, E.L.R., and A.L. prepared and characterized NC materials and films; G.G. performed electrochemical characterization; R.J.M. performed Drude fitting and analysis; A.A., T.J.R., and D.J.M. provided guidance on experimental design and interpretation; D.J.M. designed and oversaw all aspects of the project. All authors contributed to manuscript preparation.

## ■ REFERENCES

- (1) Link, S.; El-Sayed, M. A. Spectral properties and relaxation dynamics of surface plasmon electronic oscillations in gold and silver nanodots and nanorods. *J. Phys. Chem. B.* **1999**, *103*, 8410–8426.
- (2) Liu, N.; Tang, M. L.; Hentschel, M.; Giessen, H.; Alivisatos, A. P. Nanoantenna-enhanced gas sensing in a single tailored nanofocus. *Nat. Mater.* **2011**, *10*, 631–636.
- (3) Larsson, E. M.; Langhammer, C.; Zoric, I.; Kasemo, B. Nanoplasmonic probes of catalytic reactions. *Science* **2009**, *326*, 1091–1094.
- (4) Elghanian, R.; Storhoff, J. J.; Mucic, R. C.; Letsinger, R. L.; Mirkin, C. A. Selective colorimetric detection of polynucleotides based on the distance-dependent optical properties of gold nanoparticles. *Science* **1997**, *277*, 1078–1081.
- (5) Atwater, H. A.; Polman, A. Plasmonics for improved photovoltaic devices. *Nat. Mater.* **2010**, *9*, 205–213.
- (6) Gilstrap, R. A.; Capozzi, C. J.; Carson, C. G.; Gerhardt, R. A.; Summers, C. J. Synthesis of a nonagglomerated indium tin oxide nanoparticle dispersion. *Adv. Mater.* **2008**, *20*, 4163–4166.
- (7) Choi, S.; Nam, K. M.; Park, B. K.; Seo, W. S.; Park, J. T. Preparation and optical properties of colloidal monodisperse and highly crystalline ITO nanoparticles. *Chem. Mater.* **2008**, *20*, 2609–2611.
- (8) Kanehara, M.; Koike, H.; Yoshinaga, T.; Teranishi, T. Indium tin oxide nanoparticles with compositionally tunable surface plasmon resonance frequencies in the near IR region. *J. Am. Chem. Soc.* **2009**, *131*, 17736–17737.
- (9) Luther, M. J.; Jain, P. K.; Ewers, T.; Alivisatos, A. P. Localized surface plasmon resonance arising from free carriers in doped quantum dots. *Nat. Mater.* **2011**, *10*, 361–366.
- (10) Dorfs, D. et al. Reversible Tunability of the Near-Infrared Valence Band Plasmon Resonance in Cu<sub>2-x</sub>Se Nanocrystals. *J. Am. Chem. Soc.* **2011**, *133*, 11175–11180.
- (11) Wang, C.; Shim, M.; Guyot-Sionnest, P. Electrochromic nanocrystal quantum dots. *Science* **2001**, *291*, 2390–2392.
- (12) Guyot-Sionnest, P.; Wang, C. Fast voltammetric and electrochromic response of semiconductor nanocrystal thin films. *J. Phys. Chem. B* **2003**, *107*, 7355–7359.
- (13) Ung, T.; Giersig, M.; Dunstan, D.; Mulvaney, P. Spectroelectrochemistry of Colloidal Silver. *Langmuir* **1997**, *13*, 1773–1782.
- (14) Novo, C.; Funston, A. M.; Gooding, A. K.; Mulvaney, P. Electrochemical Charging of Single Nanorods. *J. Am. Chem. Soc.* **2009**, *131*, 14664–14666.

- (15) Boltasseva, A.; Atwater, H. A. Low-Loss Plasmonic Metamaterials. *Science* **2011**, *331*, 290.
- (16) Yamada, N.; et al. Donor compensation and carrier-transport mechanism in tin doped In<sub>2</sub>O<sub>3</sub> films studied by means of conversion electron <sup>119</sup>Sn Mossbauer spectroscopy and hall effect measurement. *Jpn. J. Appl. Phys.* **2000**, *39*, 4158–4163.
- (17) Zarghami, M. H.; et al. P-Type PbSe and PbS quantum dot solids prepared with short chain acids and diacids. *ACS Nano* **2010**, *4*, 2475–2585.
- (18) Ederth, J.; Heszler, P.; Hultaker, A.; Niklasson, G. A.; Granqvist, C. G. Indium tin oxide films made from nanoparticles: Models for the optical and electrical properties. *Thin Solid Films* **2003**, *445*, 199–206.
- (19) Solieman, A.; Aegerter, M. A. Modeling of optical and electrical properties of In<sub>2</sub>O<sub>3</sub>:Sn coatings made by various techniques. *Thin Solid Films* **2005**, *502*, 205–211.
- (20) Ghosh, S. K.; Pal, T. Interparticle coupling effect on the surface plasmon resonance of gold nanoparticles: From theory to application. *Chem. Rev.* **2007**, *107*, 4797–4862.
- (21) Halas, N. J., Lal, S., Chang, W.-S., Link, S. & Nordlander, P. Plasmon in strongly coupled metallic structures. *Chem. Rev.* **2011**, *111*, 3913–3961.
- (22) Zum Felde, U.; Haase, M.; Weller, H. Electrochromism of highly doped nanocrystalline SnO:Sb. *J. Phys. Chem. B* **2000**, *104*, 9388–9395.
- (23) Pflughoefft, M.; Weller, H. Spectroelectrochemical analysis of the electrochromism of antimony-doped nanoparticulate tin-dioxide electrodes. *J. Phys. Chem. B* **2002**, *106*, 10530–10534.
- (24) Feiganbaum, E.; Diest, K.; Atwater, H. A. Unity-order index change in transparent conducting oxides at visible frequencies. *Nano Lett.* **2010**, *10*, 21112116.
- (25) Lee, E. S. et al. Advancement in Electrochromic Windows; California Energy Commission, PIER: Lawrence Berkeley National Laboratory: Berkeley, CA, 2006; CEC-500-2006-052 .
- (26) Baetens, R.; Jelle, B. P.; Gustavsen, A. Properties, requirements and possibilities of smart windows for dynamic daylight and solar energy control in buildings: A state-of-the art review. *Sol. Energy Mater. Sol. Cells* **2010**, *94*, 87–105.
- (27) In fact, there is some suggestion in the literature that NiO-based electrochromic films may in some cases operate on pseudocapacitive principles. For example, see: Lee, S. E.; Tracy, C. E.; Yan, Y.; Pitts, J. R.; Deb, S. K. Solid state nanocomposite electrochromic pseudocapacitors. *Electrochem. Solid-State Lett.* **2005**, *8*, A188–A190.

#### ■ NOTE ADDED AFTER ASAP PUBLICATION

This article was published ASAP on August 25, 2011. Figure 3 and the Supporting Information have been modified. The corrected version was posted on September 1, 2011.